# Lamb wave dispersion time-domain study using a combined signal processing approach

P. Ochôa & R.M. Groves
*Aerospace NDT Laboratory, Faculty of Aerospace Engineering, TU Delft, Delft, The Netherlands*

R. Benedictus
*Structural Integrity & Composites, Faculty of Aerospace Engineering, TU Delft, Delft, The Netherlands*

ABSTRACT: Ultrasonic Lamb wave techniques are described as one of the most encouraging developments for structural health monitoring of aerospace composite structures. The reliability of those techniques is highly dependent on the quality of signal processing algorithms capable of extracting useful information out of complex responses. When damage localization is involved, it is crucial to rigorously determine time-of-flight (TOF) of wave groups. Among the available methods for automated TOF extraction the Akaike Information Criterion (AIC) and the Hilbert Transform (HT) have become very popular. The first one detects the onset-time of a signal based on the minimization of the AIC function. The second one relies on the HT to define the response envelope, allowing maximum amplitude points to be used for time interval measurement. This paper focuses primarily on comparing the aforementioned methods in order to assess their reliability for TOF determination. Additionally, a combined AIC-HT approach is used to further quantify Lamb wave dispersion phenomena.

## 1 INTRODUCTION

The long-term success of composite materials as first choices for aircraft primary structures depends on how strongly they adhere to the airworthiness regulations. A major step towards this is the installation of reliable, automated structural health monitoring (SHM) systems (Wenk & Bockenheimer 2014) in order to cope with the brittle-type behavior which, in the presence of barely-visible impact damage, may lead to unexpected failure under fatigue loading (Schijve 2004).

Some of the solutions already in operation rely on the long-range capabilities of active interrogation of ultrasonic guided waves, (Wenk & Bockenheimer 2014) as they are "*one of the most encouraging tools for quantitative identification of damage in composite structures*" (Su *et al*. 2006). One of the key missions of SHM systems is the localization of damage or detected events (SAE ARP6461 2013), making time-of-flight (TOF) a crucial parameter to be determined for acousto-ultrasonic applications. TOF can be defined as "*the time consumed for a specific wave mode to travel a certain distance*" (Su & Ye 2009). Some authors have explored this definition by computing the difference between onset times of signals. In these cases the focus was placed on identifying the first instant when a specific criterion for the separation of noise and desired signal was met. The simplest approach is to assign the onset to the point where a pre-defined fixed amplitude threshold is crossed (Gagar *et al*. 2013, Tong 1996). Although effective, the reliability of this technique is easily compromised by the existence of noise or other acoustic phenomena, and it requires trial-and-error tuning. A more robust approach is possible by using a dynamic threshold, which is adapted to the probability of signal occurrences (Youm & Kim 2003). In any case, all the aforementioned techniques cannot avoid relying on some pre-tuned parameters. Other techniques make use of mathematical formulations, such as autoregressive models. The quality of the fit of a fixed-order stationary autoregressive model to a dataset can be measured by the Akaike Information Criterion (AIC) function (Kitagawa & Akaike 1978). If the signal is windowed in a region where the onset certainly exists, then the global minimum of the AIC function indicates the point at which that signal portion can be best divided into the two different stationary segments, i.e. the onset. This principle has been widely used to develop automatic onset pickers for seismic and acoustic emission applications (Carpinteri *et al*. 2012, Kurz *et al*. 2005, Niccolini *et al*. 2012, Sedlak *et al*. 2013, Sedlak *et al*. 2009, Zhang *et al*. 2003).

From a signal processing point of view, the previous definition can, in some circumstances, be extended to a broader one according to which TOF time interval relates to a specific signal feature. Hilbert transform (HT) can be applied to the signal and

the absolute value of the resulting complex amplitude defines the signal envelope. Then, by picking the point of maximum amplitude (Liu *et al*. 2013) of the first wave group from different sensors and computing the time difference between them (Bao 2003, Su & Ye 2009) TOF can be measured. However, if dispersion is strongly present it may induce a shift in the relative position of the maximum amplitude point of the first wave group, affecting the reliability of this approach. Moreover, if other modes and reflections overlap, the extraction of the peak itself might even be erroneous.

Therefore the purpose of this article is primarily to compare the AIC and HT methods for automatic TOF determination and to establish the limits of validity of the second one. Additionally, the combination of the HT method with a dynamic threshold algorithm for wave group boundary estimation is described and tested for quantifying Lamb wave dispersion.

## 2 ALGORITHMS

### 2.1 *AIC picker*

When analyzing a time series it is possible to model the series by using a stationary autoregressive process composed of a backward-deterministic segment, and a non-deterministic segment which is considered to be Gaussian white noise and uncorrelated to the deterministic part (Kitagawa & Akaike 1978, Maeda 1985).

The fit of an autoregressive model to a dataset varies with the process order, and its quality can be evaluated by applying the maximum likelihood estimation to the modelled time series (Kitagawa & Akaike 1978). The solution is an expression that establishes the Akaike Information Criterion (AIC). According to it, the lower the AIC function value, the more adequate is the autoregressive process order and the better is the fit to a dataset. For a fixed order, the AIC function can be written for a signal window (portion) as in Equation 1 (Maeda 1985), and its global minimum indicates the point of optimal separation between the deterministic and non-deterministic segments.

$$AIC(k_w) = k_w \log\left\{\mathrm{var}\left(x[1,k_w]\right)\right\} + (n_w - k_w)\log\left\{\mathrm{var}\left(x[k_w+1,n_w]\right)\right\} \quad (1)$$

where subscript $w$ = chosen window; $n_w$ = last sample point of chosen window; $k_w$ = sample point between 1 and $n_w$; and *var* = variance of the function.

By definition the AIC function is conditioned by the window to which it is applied. If the window is chosen so that the signal onset is contained therein, then the global function minimum will correspond to the signal onset point, to a certain accuracy level. That accuracy is strongly dependent on the distribution of the deterministic and non-deterministic segments within the window. Therefore the window choice must be guided by a framing operation.

In order to tackle these problems in an optimal way it was decided to combine and adapt the approaches used by Carpinteri *et al*. (2012), Kurz *et al*. (2005), Niccolini *et al*. (2012), Sedlak *et al*. (2009) and Sedlak *et al*. (2013), keeping in mind that a trade-off between accuracy and computation time must be achieved. The squared-normalized HT envelope (see section 2.2) is used to guide the framing operation. In the definition of the envelope, the HT part is a version of the signal with a phase shift of π/2. When computing the absolute value this shift produces a positive numerical anomaly at the first sample points. Thus, the framing is performed by placing the window start some thousands of samples after the beginning of the recorded signal, and the window end right after the first wave-packet maximum (Sedlak *et al*. 2009) making sure it is positioned after the window start. This approach allows the algorithm to avoid placing the window end before the window start. Furthermore, it aims at minimizing the influence of later wave-packets so that the stationary autoregressive model fits better to the data series and the AIC method performance is maximized. After framing the window the AIC function is calculated for each sample point, and the global minimum is determined and returned as the picked signal onset.

### 2.2 *HT envelope picker*

The other implemented algorithm makes use of the squared-normalized signal envelope to determine the maximum amplitude point of the first wave group after the onset. First the signal envelope is extracted by calculating the absolute value of the complex amplitude of the Hilbert transformed signal (Equations 2 and 3). Then the square of the envelope is divided by its own absolute maximum value in order to obtain the squared-normalized envelope, which is much more sensitive to changes or singularities in the signal.

$$H\{x(t)\} = \frac{1}{\pi}\lim_{R\to\infty}\int_{-R}^{R}\frac{x(\tau)}{t-\tau}d\tau \quad (2)$$

$$Env(t) = \sqrt{x(t)^2 + H\{x(t)\}^2} \quad (3)$$

The position of the first group peak is extracted by searching for the points which correspond to zero-crossings of the first derivative of the envelope, are above a pre-defined minimum threshold amplitude, and have a relevant level difference (*Ldiff*) rel-

ative to the surrounding data defined as a quarter of the difference between the maximum and the minimum amplitudes of the envelope. By doing so for each recorded channel it is possible to compute the time differences between first group peaks in order to arrive at TOF measurements.

### 2.3 *Group boundary estimation*

The extraction of useful information from Lamb wave signals is strongly dependent on the correct interpretation of modes and groups, a task that can be assisted by determining their boundaries in the time-domain, which is something not fully explored in the literature related to Lamb wave interrogation.

The adopted approach for group time-boundary estimation is conceptually simple, light in implementation and as general as possible. The idea behind the algorithm is to link the end of a group to the global minimum between each two consecutive wave packets in the signal envelope. For that it is first necessary to determine the total amount of relevant groups and their locations. A fixed threshold peak detection method would result in either too few or too many findings. In this case it is crucial to select the relevant peaks after the signal onset. Instead of assigning an expression to model the behavior of the threshold during the peak finding process (Dimou *et al*. 2005, Youm & Kim 2003), the fixed-threshold sub-routine described in sub-section 2.2 is used recursively to always search for the first relevant peak in an envelope whose starting point is dynamically updated to a point immediately after the previous group peak. Since the envelope is adapted in each iteration, also *Ldiff* is (indirectly) adapted, creating a (pseudo) dynamic threshold algorithm which is allowed to run until a maximum of 20 peaks is identified or the end of the recorded signal is reached. After this process, each group boundary can be captured by searching for the global minimum between consecutive group peaks using the same fixed-threshold sub-routine (sub-section 2.2).

## 3 EXPERIMENTS

It was decided to conduct the experiments on a panel made from aluminum alloy 6082, in order to isolate the time-domain variables from attenuation and dispersion as much as possible. The dimensions of the panel were 900 × 1500 × 1.5 $mm^3$, so that the wave propagation length would be enough to test the limits of validity of the second method.

A five-cycle ultrasonic Hanning windowed tone-burst was produced by an Agilent 33500B Series waveform generator, and transmitted to the plate through a Physical Acoustics WSα Series piezoelectric transducer (actuator) placed 200 mm away from the edge of the panel at the middle of the width. The Lamb wave response was sensed also by a Physical Acoustics WSα Series piezoelectric transducer (sensor 1) whose position was varied from 200 to 1000 mm away from the actuation point, with increments of 200 mm (positions $x_1$ to $x_5$) always measured collinearly with the actuator and parallel to the length of the panel. The coupling of both transducers to the plate was ensured by Sonotech shear gel and adhesive tape. The sensed signals were conditioned in a Thurlby Thandar Instruments WA301 wideband amplifier with a gain of ten times, and acquired via a PicoScope 6402A digital oscilloscope, as depicted in Figure 1.

The excitation amplitude was set to 10 $V_{pp}$, and the center frequency to 250, 500 and 750 kHz, allowing three different dispersion states to be tested for each sensor 1 position.

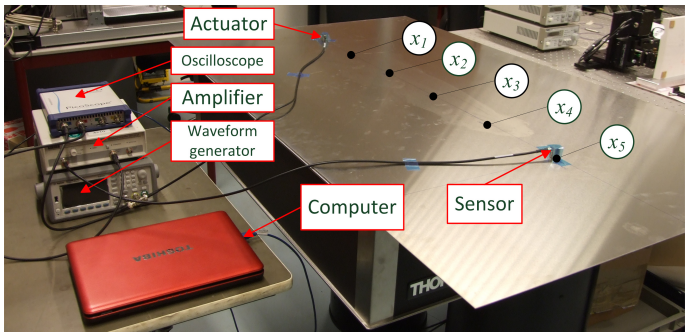


Figure 1. Experimental set-up: equipment and sensor positions.

## 4 RESULTS AND DISCUSSION

### 4.1 *TOF analysis*

In order to minimize computation time and keep statistical relevance it was decided to analyze the first five waveforms of each set of 32 extracted at each sensor position, for each frequency. The five different sensor 1 configurations enabled the extraction of the TOF for four different propagation distances: $TOF_{12}$ for $d_{12} = |x_1 - x_2|$, $TOF_{13}$ for $d_{13} = |x_1 - x_3|$, $TOF_{14}$ for $d_{14} = |x_1 - x_4|$, and $TOF_{15}$ for $d_{15} = |x_1 - x_5|$.

After computing the signal onset and the time of the first wave-packet peak for each of the analyzed waveforms, the difference between corresponding points was taken to arrive at each of those TOFs. The obtained values were then used to calculate the $S_0$ Lamb mode group velocity at each tested frequency. As shown in Figure 2 the results from the two methods reveal good agreement between them, except for 500 kHz where they differ by 220 m/s.

Overall, the experimental points present an acceptable agreement with the theoretical curve. However, they only allow a very limited evaluation of the performance of the two algorithms. Hence it was decided to plot the difference of group velocity ($\Delta v_g$) obtained with each algorithm as a function of propa-

gation distance, for each excitation frequency (Figure 3). Two main observations can be made from the chart. Firstly, there is a clear steady decrease in $\Delta v_g$ with increasing distance for all frequencies, indicating consistency of both methods when applied to $S_0$ mode analysis. This was expected, since at larger distances the two zero-order modes are more clearly separated and the peak of the (not so dispersive) $S_0$ mode can be more unambiguously detected. Secondly, while the curves for 250 and 750 kHz are relatively close to each other (especially after 200 mm), almost all the points for 500 kHz are at least 150 m/s above the others.

The reason for this discrepancy at 500 kHz can be better understood by looking at Figures 4 and 5, where the relative error of the TOF results from the AIC and HT envelope algorithms (respectively) are plotted as a function of propagation distance, for each frequency.

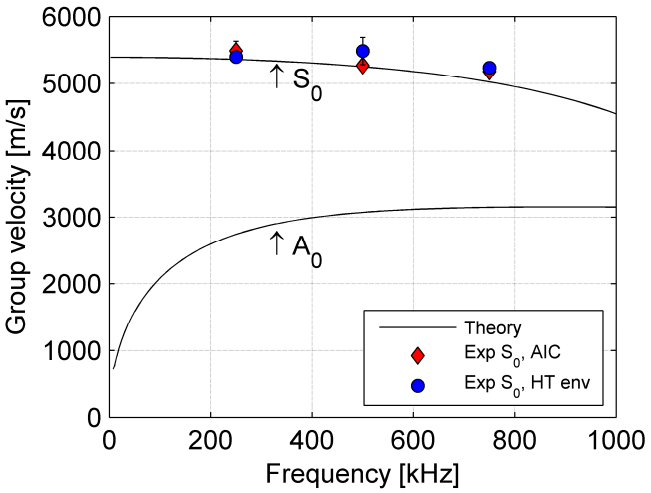


Figure 2. Group velocity dispersion curves for the aluminum panel (computed with DISPERSE™ software).

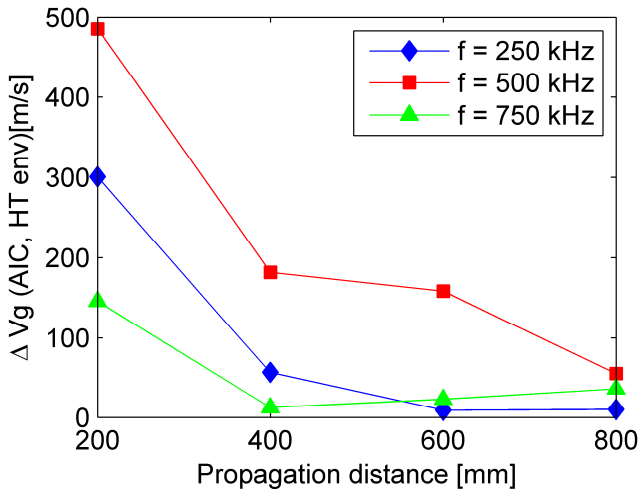


Figure 3. Variation of the $S_0$ group velocity difference between methods with distance, for each excitation frequency.

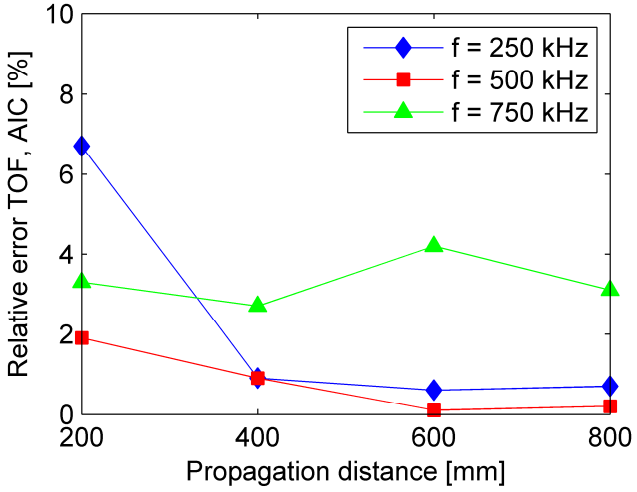


Figure 4. Variation of the relative error of the AIC results with distance, for each excitation frequency.

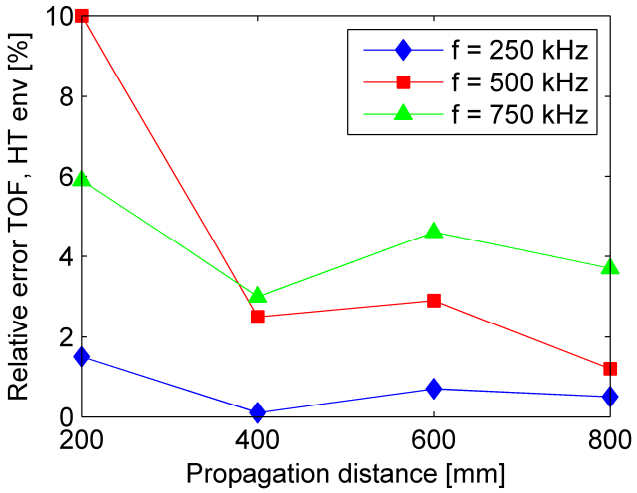


Figure 5. Variation of the relative error of the HT envelope results with distance, for each excitation frequency.

In both graphs the relative error falls within the same range of values for 250 and 750 kHz at all distances except at 200 mm (see discussion about relative error in the AIC algorithm results on the next page), corroborating the proximity of the $\Delta v_g$ curves for these two frequencies. However, in Figure 4 the relative error for 500 kHz is always below 2%, while in Figure 5 it starts at 10% and only goes below 2% at 800 mm. Thus, the discrepancy of $\Delta v_g$ for this particular frequency is in fact due to poorer TOF results from the HT envelope method at that frequency.

This occurrence can be explained by analyzing the first (or first two) wave-packet(s) from the signals which were captured at $x_1$ and $x_2$ for 500 kHz and used to compute the TOF for 200 mm (Figures 6 and 7). At $x_1$ (200 mm away from the actuator), the $S_0$ and $A_0$ are superimposed as it is not possible to distinguish their groups separately. As a result, their amplitude is summed, masking the position of the peaks of each mode. Therefore, the observed first wave-packet peak is not actually the $S_0$ peak. At $x_2$ (400 mm away from the actuator), it is already possible to distinguish two groups, although they are

still not completely separate. There is still mode overlapping with part of the $S_0$ mode (algebraically) summed to part of the $A_0$ mode. Therefore, at this position the first wave-packet peak approximately corresponds to the desired mode peak. Nevertheless, the subtraction of the peak times results in $TOF_{12}$ being considerably different from the theoretical value.

This phenomenon is stronger for 200 mm, but it is always present because the (more dispersive) $A_0$ mode always overlaps with part of the $S_0$. However, for 200 mm it has clearly more influence at 500 kHz. The explanation lies in the combination of two tendencies. At 250 kHz the $A_0$ group velocity is lower causing the mode to arrive late enough to be discernible, even though $x_1$ is closer to the actuation point. At 750 kHz the $A_0$ group velocity is higher causing the mode to arrive earlier. But because frequency is higher the mode duration becomes lower, making it easier to discern the presence of two groups, although not as clearly as for 250 kHz.

Previously it was pointed out that for 250 kHz at 200 mm, the results obtained with the AIC method presented a relative error of 6.7% (Figure 4). At that frequency, noise and actual signal have more similar oscillatory characteristics than in the other cases. Moreover, at $x_1$ and $x_2$, the length of the noise segment contained in the frame used for the AIC function computation is smaller than at the other points. These two factors combined make more difficult for the AIC function to reach a sharp global minimum (i.e. to clearly separate noise from actual signal), as seen by its shape in Figure 8.

To fully characterize the performance of the HT envelope method for TOF determination it is envisioned to perform a similar study for the $A_0$ mode. That can be achieved by implementing a time-scale domain mode separation algorithm based on wavelet transform (Se & Ye 2009). The possibility of installing a selective mode generation system is wittingly left aside because the reliability of that strategy can only be assured in laboratory conditions (Su & Ye 2004).

### 4.2 *Dispersion analysis*

The results from 1st wave-packet duration study proved to be inconclusive, since no clear pattern was observed with increasing propagation distance, for the tested frequencies. This was due to erroneous group end-time determination, which in turn was caused by the mode superposition effect described in the previous sub-section. Therefore, it is valid to say that mode time-boundary estimation cannot solely rely on direct HT signal envelope information. In future developments the algorithm will be improved by using time-scale domain mode separation and the combined analysis of multiple signal features.

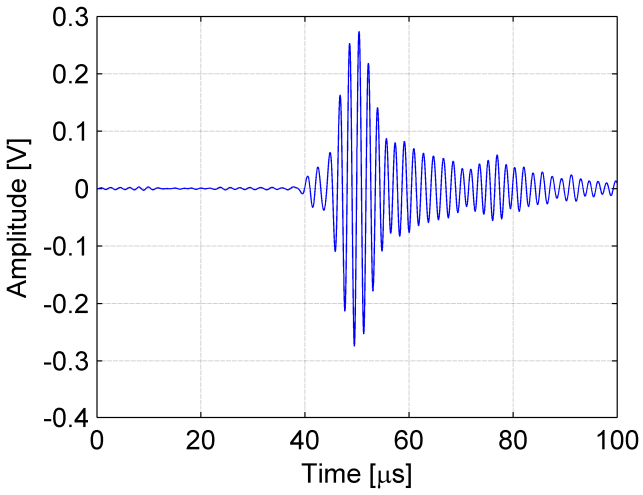


Figure 6. Part of the signal acquired at $x_1$, for 500 kHz.

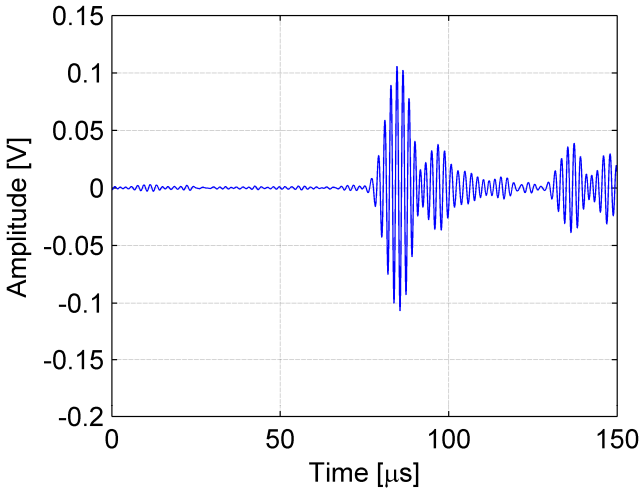


Figure 7. Part of the signal acquired at $x_2$, for 500 kHz.

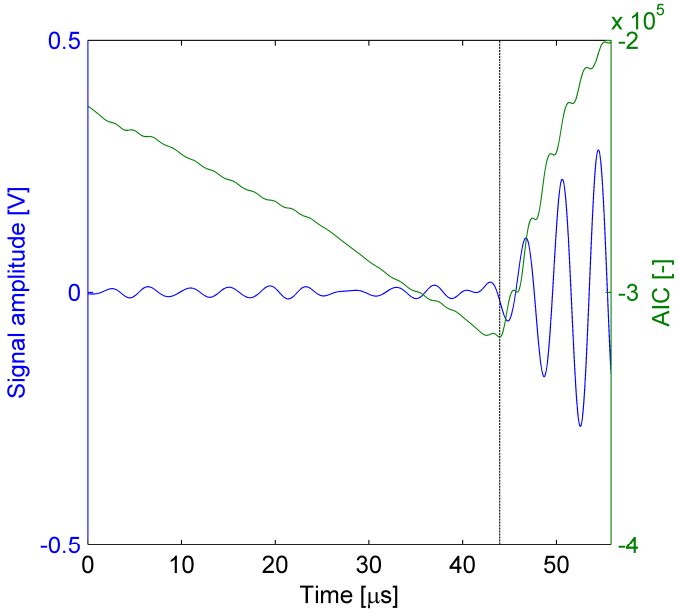


Figure 8. Determination of the signal onset with the AIC function at $x_1$ with a 250 kHz excitation frequency.

## 5 CONCLUSIONS

This article focused primarily on the evaluation of two different methods for TOF measurement, irrespectively of the propagation medium material.

The combined use of the HT envelope for guiding the signal window selection in the AIC algorithm proved to be of value for the extraction of consistent and reliable TOF results. The performance of the AIC-HT method is expected to be unaffected by the stronger dispersive properties of composite materials.

The optimization of the capabilities of the combined AIC-HT method for SHM relies on the use of effective signal filtering, adaptable framing operations, and advanced programming techniques to make the algorithm computationally more efficient. If this is achieved, it is an algorithm with a high level of accuracy and a strong potential for integration.

After this study it is valid to state that the HT envelope method can be reliably used, with computational efficiency advantages, for TOF analysis of weakly dispersive Lamb modes (e.g. $S_0$), as long as mode separation is previously performed by applying some extra signal processing (e.g. time-scale domain analysis with wavelet transform).

The use of the HT envelope method for the TOF analysis of strongly dispersive Lamb modes (e.g. $A_0$) is dependent on the accuracy of predictions of the dispersion effect in order to compensate for the time spreading of the mode. This case is still to be tested and is expected to provide additional information on the performance of the HT envelope method when applied to TOF measurement in composite materials (i.e. highly dispersive media).

## REFERENCES


Bao, J. 2003. Lamb wave generation and detection with piezoelectric wafer active sensors. *PhD Thesis*, University of South Carolina.

Carpinteri, A., Xu, J., Lacidogna, G. & Manuello, A. 2012. Reliable onset time determination and source location of acoustic emission in concrete structures. *Cement & Concrete Composites* 34: 529-537.

Dimou, A. Nemethova, O. & Rupp, M. 2005. Scene change detection for H.264 using dynamic threshold techniques. In *Proceedings of 5th EURASIP Conference on Speech and Image Processing, Multimedia Communication and Service, June 29 - July 2 2005, Slovak Republic*.

Gagar, D., Martinez, M., Yanishevsky, M., Rocha, B., McFeat, J., Foote, P. & Irving, P. 2013. Detecting and Locating Fatigue Cracks in a Complex Wing-Box Structure Using the Acoustic Emission Technique: A verification Study. In Fu-Kuo Chang (ed.), *Structural Health Monitoring 2013 - A Roadmap to Intelligent Structures; Proc. 9th Intern. Workshop on SHM, Stanford, 10-12 September 2013*. Lancaster: DEStech Publication, Inc.

Kitagawa, G. & Akaike, H. 1978. A procedure for the modeling of non-stationary time series. *Ann. Inst. Statist. Math.* 30 (Part B): 351-363.

Kurz, J.H., Grosse, C.U. & Reinhardt, H.W. 2005. Strategies for reliable automatic onset time picking of acoustic emissions and of ultrasound signals in concrete. *Ultrasonics* 43: 538-546.

Liu, P., Groves, R.M. & Benedictus, R. 2013. Signal processing in optical coherence tomography for aerospace material characterization. *Optical Engineering* 52(3), 033201, 1-7.

Maeda, N. 1985. A method for reading and checking phase times in auto-processing system of seismic wave data. *Zisin* 38: 365-379.

Niccolini, G., Xu, J., Manuello, A., Lacidogna, G. & Carpinteri, A. 2012. Onset time determination of acoustic and electromagnetic emission during rock fracture. *Progress In Electromagnetics Research Letters* 35: 51-62.

SAE ARP6461. 2013. Guidelines for Implementation of Structural Health Monitoring on Fixed Wing Aircraft.

Schijve, J. 2004. *Fatigue of Structures and Materials*. Dordrecht: Kluwer Academic Publishers.

Sedlak, P. Hirose, Y. & Enoki, M. 2013. Acoustic emission localization in thin multi-layer plates using first-arrival determination. *Mechanical Systems and Signal Processing* 36: 636-649.

Sedlak, P., Hirose, Y., Khan, S.A., Enoki, M. & Sikula, J. 2009. New automatic localization technique of acoustic emission signals in thin metal plates. *Ultrasonics* 49: 254-262.

Su, Z. & Ye, L. 2004. Selective generation of Lamb wave modes and their propagation characteristics in defective composite laminates. In *Proceedings of the Institution of Mechanical Engineers, Part L: Journal of Materials: Design and Application* 218 (2): 95-110

Su, Z. & Ye, L. 2009. *Identification of Damage Using Lamb Waves: From Fundamentals to Applications*. In Pfeiffer, F. & Wriggers, P. (eds), *Lecture Notes in Applied and Computational Mechanics* 48. Springer.

Su, Z., Ye, L. & Lu, Y. 2006. Guided Lamb waves for identification of damage in composite structures: A review. *Journal of Sound and Vibration* 295: 753-780.

Tong, C. & Kennet, B.L.N. 1996. Automatic Seismic Event Recognition and Later Phase Identification for Broadband Seismograms. *Bulletin of the Seismological Society of America* 86(6):1896-1909.

Wenk, L. & Bockenheimer, C. 2014. Structural Health Monitoring: A real-time on-board 'stethoscope' for Condition-Based Maintenance. In *Airbus technical magazine, Flight Airworthiness Support Technology* 54: 22-29.

Youm, S. & Kim, W. 2003. Dynamic threshold method for scene change detection. In *Proceeding of Intern. Conf. Multimedia and Expo* 2: 337-340, 6-9 July 2003.

Zhang, H, Thurber, C. & Rowe, C. 2003. Automatic P-Wave Arrival Detection and Picking with Multiscale Wavelet Analysis for Single-Component Recordings. *Bulletin of the Seismological Society of America* 93(5): 1904-1912.